Composites Communications 57 (2025) 102448

Contents lists available at ScienceDirect

Composites Communications

journal homepage: www.elsevier.com/locate/coco

Research article

Enhancing the electrical conductivity of TPU-TPU/SWCNT multilayered composites using melt multipliers

Mariana Martins da Silva [a,*,1], Rui Ribeiro [a], Ana Sofia Oliveira [a,2], Mariana Paiva Proença [b], Maria Conceição Paiva [a], José António Covas [a,*]

[a] Institute for Polymers and Composites, University of Minho, Campus of Azurém, Guimarães, 4800-058, Portugal
[b] ISOM and Departamento de Electrónica Física, Universidad Politécnica de Madrid, Ava. Complutense 30, Madrid, E-28040, Spain

ARTICLE INFO

Keywords:
Single-walled carbon nanotubes
Thermoplastic polyurethane
Melt multipliers
Multilayered composites

ABSTRACT

Structuring and confining polymer layers have a profound influence on material properties and have been studied as a means of achieving tailored and multifunctional materials. In this work, single-walled carbon nanotubes (SWCNT) are incorporated into thermoplastic polyurethane (TPU) using melt-mixing techniques. An electrical percolation threshold at 0.6 wt.% SWCNT is achieved in melt-extruded filaments after pre-dispersing SWCNT in polypropylene glycol. Additionally, a prototype device composed of a series of small-scale layer multipliers is developed. The application of the baker's transformation enabled the extrusion of tapes with alternating layers of two different melts, TPU and composite TPU with SWCNT. These layered structures, obtained using an increasing number of melt multipliers, are characterized in terms of morphology, mechanical, and electrical properties. We demonstrate that layered tapes of TPU with TPU/SWCNT preserve the electrical conductivity of the TPU/SWCNT composite, at half SWCNT weight percentage, and the ductility of neat TPU.

1. Introduction

The outstanding properties of carbon nanotubes (CNT) make them appealing fillers for polymer matrices as at a very low filler loading it is possible to achieve significant improvements in polymer's properties and multifunctionality. As a consequence of the conjugated π-molecular orbital that extends across the CNT structure, electron mobility is possible with CNT presenting high intrinsic electrical conductivity, reaching $\sim 10^3$ S m^{-1} [1]. Granting electrical conductivity to low density materials through the assembly of a conductive path within a polymer matrix is a popular application of CNT. CNT filled polymer composites have been explored for the development of sensors, wearable devices, shape-memory polymers, self-healing polymers, and energy storage and optoelectronic devices [2–5].

At a critical CNT concentration, the electrical conductivity of the composite rapidly increases as a conductive network is formed throughout the composite volume. Experimental works show that an electrical percolation threshold (ϕ_c) can be achieved at CNT loadings as low as 0.1 weight percentage (wt.%) due to their high aspect ratio [6,7]. However, the high viscosity of thermoplastic polymers, combined with the strong van der Waals forces between CNT that stabilize their agglomerate form and the weak interface adhesion of CNT, hinders obtaining a ϕ_c at very low loadings [6]. The ϕ_c in thermoplastic matrix composites usually lies between 0.2 and 15 wt.% of CNT content [8]. Enhancing CNT's solubility/reactivity toward the polymer through surface modifications and purification, as well as the use of compatibilizers [4,7,9,10], are common strategies to improve their dispersion.

Selecting appropriate processing methods is also crucial to obtaining a proper dispersion/distribution of the filler. Reducing polymer's viscosity by processing composites through solvent casting, or by mixing the CNT with the monomers prior to *in situ* polymerization, often aids in achieving good results. These methods are, nevertheless, time consuming and rely on the use of solvents, which makes them a poor fit in pursuit of sustainable options for large scale production. In comparison, melt-mixing techniques based on the mechanical mixing of the filler with a polymer in the melt state do not require the use of solvents and are well-suited for industrial production. Applying high shear and/or extensional stresses during a sufficient amount of time is required to disperse fillers down to the nanoscale, which may be enhanced by strong adhesion between filler and polymer matrix. However, these methods are less efficient in achieving optimal results [11]. Elastomers

* Corresponding authors.
E-mail addresses: mmsilva@dep.uminho.pt (M. Martins da Silva), jcovas@dep.uminho.pt (J.A. Covas).
[1] Present address: School of Mechanical and Aerospace Engineering, Queen's University Belfast, BT9 5AH, Belfast, United Kingdom.
[2] Present address: Centre for Innovation in Polymer Engineering, 4800-058, Guimarães, Portugal.

https://doi.org/10.1016/j.coco.2025.102448
Received 14 February 2025; Received in revised form 18 April 2025; Accepted 7 May 2025
Available online 24 May 2025

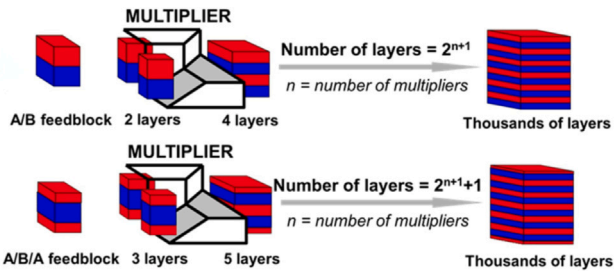

Fig. 1. Schematic illustration of layer multiplication by splitting, spreading, and stacking the melt stream [18].

filled with CNT generally present ϕ_c between 1 to 5 wt.% CNT load when produced through a melt-mixing technique [12].

Well dispersed polymer/CNT composites have been successfully prepared by a number of melt processing techniques, namely using intermeshing co-rotating twin screw extruders and intensive mixers. Less frequently adopted processing strategies, such as the assembly of hierarchical structures, may bring advantages in the design of polymer composites through selective localization of fillers and enhanced dispersion [13–17]. Forced assembly multilayer co-extrusion is a continuous and flexible melt processing route that can create layered structures based on the baker's transformation by repeatedly stretching, cutting, and stacking the melt flow [18–20]. Typically, two individual polymer melts are joined in an initial two-layered structure in a conventional co-extrusion feedblock and then flow successively through several layer multiplying elements (LME) that split and recombine the melt, thus gradually increasing the number of layers, as illustrated in Fig. 1. This confinement of polymer layers has been proven to enhance properties such as mechanical, gas barrier, optical, dielectric, and shape-memory behavior [18,21]. The layer thickness is primarily controlled by the output of each component and by the number of layers formed. Research works report a maximum of 16384 layers produced by multilayer co-extrusion [22,23], with layer thicknesses varying from microns down to the nanometer scale. A critical layer thickness exists and depends on the polymer's characteristics, with the lower thickness of 10 nm reported for layered polystyrene/poly(methyl methacrylate) films [23]. Since the baker's transformation can be executed in two distinct ways, i.e., by (i) a stretching-folding operator, which causes the middle layer to fold on itself resulting in a mirroring of the structure, or by (ii) a stretching-cutting-stacking operator, that yields higher number layers with a more uniform thickness [24], several designs of static mixers were proposed for the assembly of layered structures [25–28], as well as variations of the interfacial surface generator used for multilayer co-extrusion [29–32].

In this work, a prototype device that applies the baker's transformation using small-scale layer multiplying elements (LME) with DentIncx mixing channels [28] was designed and fabricated. One of the advantages of this approach lies in the much simpler fabrication requirements. Although the original concept was applied to injection moulding, it can be directly transposed to melt extrusion.

The dispersion of single-walled carbon nanotubes (SWCNT) in highly viscous polymers remains challenging. A lower percolation threshold may be reached when nanoparticle dispersion is carried out in solution and composites are prepared by solvent casting. However, solvents such as tetrahydrofuran and dimethylformamide, which are commonly used for thermoplastic polyurethane (TPU) processing, are known for their toxicity and adverse environmental and health impact. Under solvent-free melt-mixing conditions, the required filler loadings are typically higher than those observed for solvent casting processing methods.

In the present study, a low electrical percolation threshold was attained for SWCNT/TPU composites (in the range of 0.3 to 0.8 wt.%) prepared by melt-mixing. This was accomplished through the use of (i) pre-dispersed SWCNT in polypropylene glycol (PPG) and (ii) a static mixer. Additionally, CNT/polymer composites are stiffer than the polymer matrix due to the high modulus of the CNT and possible restrictions on polymer chain mobility. The production of alternating TPU composite/TPU layers using the static mixer reduced the stiffness, yielding a flexible material without compromising electrical properties.

The microstructure, mechanical properties, and electrical properties of the prepared tapes, with alternating layers of TPU and composite, are discussed and the feasibility of using the prototype device for advanced composite processing is evaluated.

2. Materials and methods

2.1. Materials

A melt processable ester-based thermoplastic polyurethane (TPU, Desmopan 3360 A), with a shore hardness of 62, a density of 1.154 g cm^{-3}, an ultimate tensile strength of 29 MPa, a strain at break of 754%, according to the manufacturer, and a measured melt flow index (MFI) of 8.96 g 10 min^{-1} (190 °C, 2.16 kg), was obtained from Covestro (Leverkusen, GER). Polypropylene glycol (PPG, M_W = 45 g mol^{-1}) was used as plasticizer and purchased from Acros Organics (Geel, BE). Single wall carbon nanotubes Tuball™ (SWCNT, batch 109-16092015), with ≥5 μm length and an average outer diameter of 1.6 ± 0.4 nm, from OCSiAl (Leudelange, LU), were used as conductive fillers.

2.2. Preparation of TPU nanocomposites

To maximize filler dispersion, a pre-dispersion of SWCNT in PPG was performed based on a previous work [33]. SWCNT were weighed and sonicated in ethanol in an ultrasound bath for 15 min, at room temperature. The suspension was added to PPG, and mixed with a T18 digital ULTRA-TURRAX® homogenizer (IKA, Staufen, GE), equipped with a S 18 *N* - 10G tip, for 1 h and 30 min at 1300 rpm. Three separate suspensions were prepared, with 4.5, 6.7, and 8.9 wt.% of SWCNT in PPG and used to coat TPU pellets. The dispersions were transferred to the weighted TPU pellets and stirred at 40 rpm using a IKA MINISTAR 40 (IKA, Staufen, GE) with a propeller stirrer, at room temperature, until the ethanol was fully evaporated. Three sets of coated pellets were obtained, with SWCNT wt.% compositions of 0.4, 0.6 and 0.8 wt%.

Composite filaments were obtained by melt-mixing the TPU coated pellets in a small-scale prototype modular co-rotating intermeshing twin screw extruder coupled to a circular die with a diameter of 1.75 mm, illustrated in Fig. 2. A miniaturized volumetric feeder (using a Piovan, IT, MDP1 platform) was located above the extruder hopper. The extruder screws, with an external diameter of 13 mm, were assembled with three intensive mixing zones, composed of kneading blocks (Fig. 2, in red), between conveying zones. The length-to-diameter (L/D) ratio of the extruder barrel is 27, with a 1.5 ratio of outer to inner diameter. The extrusion line consists of 5 heated barrels (Z1 to Z5 in Fig. 2), which are set to temperatures of 190 °C, 195 °C, 195 °C, 190 °C, and 185 °C, respectively, with the exit die temperature set at 170 °C. The temperature was decreased at the screw tip and die in order to increase the melt viscosity and thus obtain a more consistent filament. The screw speed was set to 85 rpm. The extrudate was cooled in a water bath located downstream and filaments were collected with the aid of a haul-off with controlled speed. Composite filaments of TPU with 9 wt.% of PPG and 0.4, 0.6, and 0.8 wt.% SWCNT, with a diameter of 2.30 mm, were obtained.

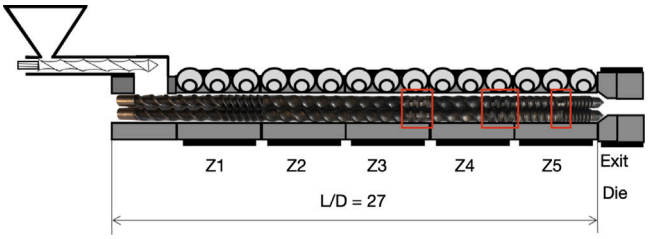

Fig. 2. Extrusion layout: the screws are composed of an initial conveying zone positioned below the feed port, followed by a first set of mixing blocks at the end of Z3. This is followed by a second conveying zone, plus an intensive mixing zone between Z4 and Z5, and a smaller mixing zone located at Z5. Circles in the barrel indicate sample collecting devices, which were not used for this work. (For interpretation of the references to color in this figure legend, the reader is referred to the web version of this article.)

Table 1
Theoretical number of layers (L_n) and individual layer thickness per LME used.

Number of LME	L_n	Layer thickness (μm)
1	8	87.5
2	32	28.9
3	128	5.47
4	512	1.38

2.3. Layer multiplication

A prototype device was designed and fabricated in order to use up to 5 multiplying elements (LME), enabling the generation of a different number of layers from two inlet melts. The LME design is based on the DentIncx mixing element [28,34], which is depicted in Fig. 3a. The two different polymer melts are repeatedly stretched and folded, combining interfaces with left and right rotational directions, and the flow is split horizontally [28]. For machining purposes, the channels are split into two halves, as represented in Fig. 3b, and when joined together, they compose one LME (Fig. 3c). The number of layers formed (L_n) can be calculated according to the following equation (Eq. (1)) [28]:

$$L_n = 2 \times 2^{2 \times n} \quad (1)$$

with n corresponding to the number of layer multiplying elements.

The fabricated prototype is presented in Fig. 4. An adapter with two pistons (A) is coupled to the motor shaft of a capillary rheometer (Davenport, from Daventest Ltd., Welwyn Garden City, UK). A barrel (B) composed of two cylindrical channels, each with a volume of 2.09 cm^3, is used to feed two different melts, and it is directly connected to a transition channel. The outlet section of this channel is square and has a cross-section of 4 mm^2. A piston speed of 7.5 mm min^{-1} generates an average shear rate of ~10 s^{-1} along the channels, thus minimizing possible interfacial stresses. The device is supported by a structure with 4 vertical screws (C) that enables the addition or removal of LME operating always at the same height. The various LME are mounted vertically (E) followed by the die (F), with a rectangular cross-section of 0.7 × 5 mm at the outlet. Table 1 presents the theoretical number of layers and their thicknesses, assuming that, at the die exit, the extruded tape will have a thickness of 0.7 mm.

To evaluate LME preliminary studies at room temperature, using common play-dough, were conducted and are presented in the supplementary material (Figure A1).

The temperature of each LME is controlled by a heater band (Figure A2) set to 190 °C to produce the layered TPU/TPU composite tapes. Neat TPU and composite TPU, with 0.6 wt.% of SWCNT and 9 wt.% of PPG (sTPU, with an MFI of 11.1 g·10 min^{-1} (190 °C, 2.16 kg), Table A1), were molded into cylinders through compression moulding, using a mold specifically designed for this purpose, at 190 °C for 5 min, with an applied pressure of 10 tons. The cylinders were weighted (1.5 g per melt charge) to ensure equal output and placed in the reservoirs of the prototype.

2.4. Characterization

2.4.1. Thermogravimetric analysis

Thermograms of melt-extruded TPU and composites were collected with a TGA Q500, from T.A. Instruments® (DE, USA), with a weighting precision of ±0.01% and 0.1 μg sensitivity. A platinum crucible was used to place the samples whose thermograms were collected at a heating rate of 10 °C min^{-1}, from 40 °C to 700 °C, under N_2 atmosphere. Three samples were measured for each of the materials/composites. Peaks of the derivative curves were determined with the OriginPro® 2024 (10.1.0.170) software.

2.4.2. Mechanical properties

Films with 600 μm thickness of TPU and of composite filament of TPU with 0.6 wt.% SWCNT and 9 wt.% of PPG were made through hot compression moulding, at 190 °C, under a pressure of 20 tons. Rectangular samples were cut from the compression moulded films and the extruded tapes, with an approximate length of 30 mm and 5 mm width. Samples were tensile tested with an Autograph AGS-X Series from Schimadzu Corporation (Kyoto, JP), equipped with a 1 kN cell and a video extensometer with a f2.5 lens, from Schimadzu. The test was performed at an initial speed of 5 mm min^{-1} to determine the Young's modulus, and at 50 mm min^{-1} after 0.5% deformation. The gauge length was set at 10 mm and the grip distance was 20 mm. Young's modulus (E) was determined from the linear fit in the deformation range of 0.2 - 0.5%, with the Trapezium X software. Three samples of each material were analyzed, except for TPU/$sTPU_1$, with only one measured sample.

2.4.3. Electrical resistivity measurements

Electrical resistivity measurements were carried out with a Keithley SMU 2635B SourceMeter® from Keithley Instruments Inc. (Cleveland, OH, USA). Volume resistivity measurements were made at room temperature directly on the extrudate filaments (~2.30 mm diameter) and layered tapes (~0.7 mm thickness and ~5 mm width). The electrodes were placed at a distance of ~8 mm. KickStart 2 software was used to record current–voltage (I-V) curves acquired under direct current (DC) on a source range of 20 V (from −10 V to 10 V with 0.5 V step). A linear fit was applied to calculate the resistance as the inverse of the I-V curve slope. Volume conductivity (σ_{DC}) was obtained through Ohm's law. Five samples were tested for each composite. A Kruskall–Wallis test was conducted to assess statistically significant differences between the medians of different composites.

2.4.4. Optical microscopy

Optical microscopy (OM) images were obtained with a Leica DM2500 P microscope equipped with a digital camera Leica DMC2900. Transversal sections of 3 μm thickness were cut with an ultramicrotome (Leica UC6) equipped with a cryogenic chamber at −90 °C. The LAS X software was used to record the images, and the ImageJ (1.53a) software [35] to determine layer thickness and agglomerate areas for the collected samples. A total area of ~0.6 mm^2 was analyzed for each composite, measuring the agglomerate areas greater than 2 μm^2.

2.4.5. Scanning electron microscopy

The morphology of the cross-section of composites was observed by SEM (Nano SEM–FEI Nova 200), with an integrated EDAX–Pegasus X4M at high vacuum (1.0 nm at 15 kV resolution), a TDL, and ETD detectors. Samples were immersed in liquid N_2 and cryofractured, before coating with Au-Pd (80-10 wt%).

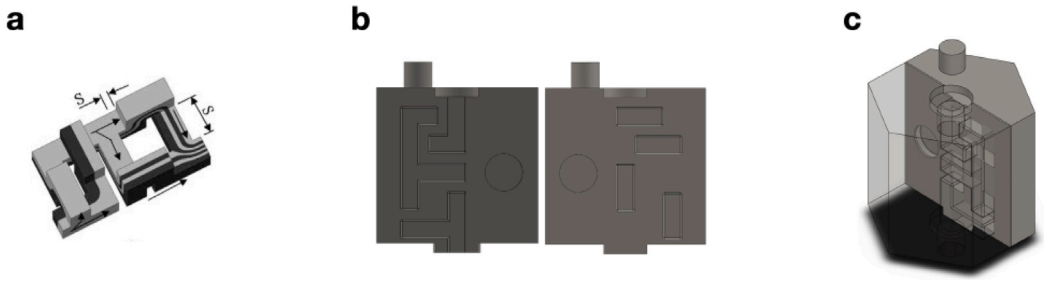

Fig. 3. Layer multiplying element (LME): (a) Basic unit element of the splitting serpentine geometry, the DentIncx mixer [28]; (b) two halves of one LME, depicting the channel's geometry; (c) one LME of the modular prototype device.

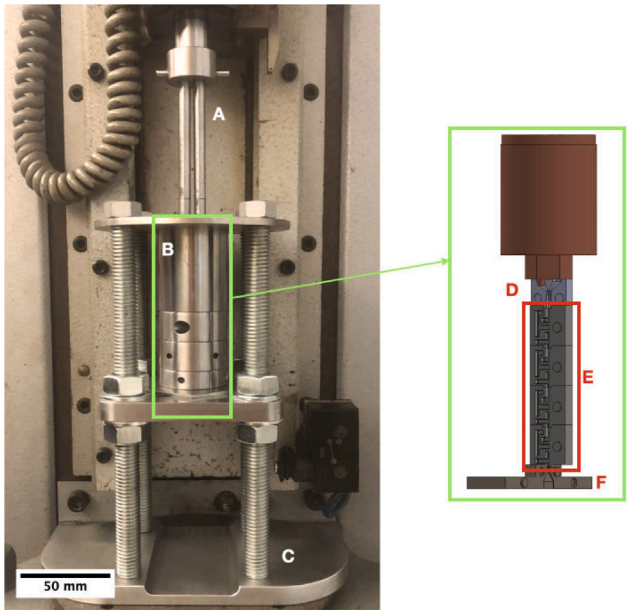

Fig. 4. Prototype device capable of producing extrudates from two inlet melts. The pistons (A) are coupled to the motor of a capillary rheometer, which determines the velocity of the flow, and forces the materials to exit the deposit (B). The device is supported by a structure with 4 vertical screws (C). Materials leaving the deposit enter the transition channel (D), which leads to the LME (E). Material can be collected in the form of a tape after passing through the exit die (F).

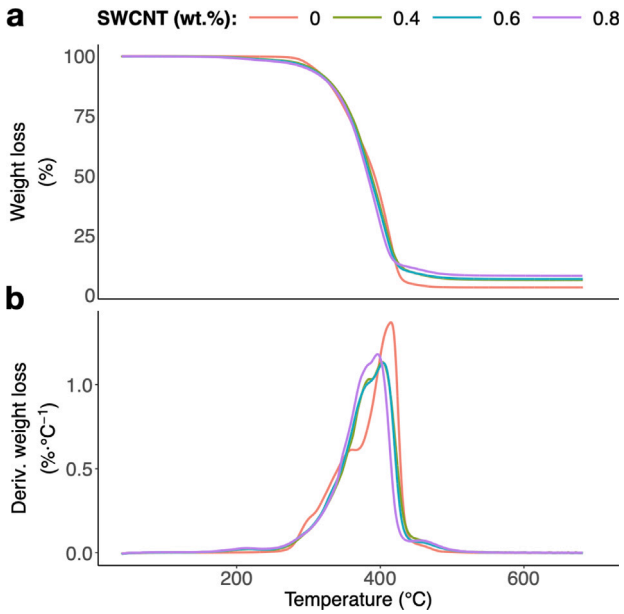

Fig. 5. Representative (a) thermograms and (b) derivatives of weight loss of melt-extruded composites and neat TPU. (For interpretation of the references to color in this figure legend, the reader is referred to the web version of this article.)

2.4.6. Atomic force microscopy

Atomic Force Microscopy (AFM) images were obtained with a Nano-observer from Concep Scientific Instruments (Paris, France), using a conductive silicon probe coated with Pt-Ir, with a spring constant of 3 N m^{-1}, and a frequency of 65 kHz, capable of operating both in resonant and High Definition Kelvin Force Microscopy (HD-KFM) mode. The images were processed with the Gwyddion 2.66 software.

2.4.7. Statistical analysis and data visualization

Statistics and data visualization were performed in OriginPro® 2024 (10.1.0.170) software and RStudio (2023.12.0.369) [36], with R version 4.2.3; dplyr [37] and tidyverse [38] packages were used to treat data, and plots were created with the ggplot2 [39] package.

3. Results and discussion

3.1. Melt-extruded composite filaments

Thermograms of the melt-extruded composites and neat TPU are displayed in Fig. 5. Composites are stable up to ~220 °C, whereas neat TPU is thermally stable up to ~280 °C. The small peak above 200 °C, observed for the derivative of the TGA curve of the TPU composites, may be attributed to vaporization of the PPG remaining in the composite (not present in pure TPU). The weight loss at 250 °C for all the samples is presented in Table 2, showing a difference of approximately 2% in weight loss for the composites relative to TPU. This indicates that part of the PPG was already vaporized during composite preparation by melt mixing.

Table 2
Weight losses at 250 °C (WL_{250}) and 700 °C (WL_{700}), and temperature at which degradation reaches its maximum rate (DTG_{max}) of neat TPU and melt-extruded composites.

TPU	SWCNT	PPG (wt.%)	WL_{250}	WL_{700}	DTG_{max} (°C)
100	0	0	0.2 ± 0.2	96.7 ± 0.3	410 ± 6
90.6	0.4	9	1.5 ± 0.1	93.5 ± 0.5	401 ± 2
90.4	0.6	9	1.5 ± 0.2	92.9 ± 0.6	403 ± 3
90.2	0.8	9	2.2 ± 0.2	92.0 ± 0.2	397 ± 2

Two large degradation peaks are observed for all samples (Fig. 5b), related to the decomposition of TPU hard and soft segments. The temperature at which the degradation reaches its maximum is registered in Table 2 (DTG_{max}), decreasing nearly 10 °C with the addition of both PPG and SWCNT.

Scanning electron microscopy (SEM) micrographs of the neat TPU and composite filaments, with different SWCNT wt.% and at different magnifications, are presented in Fig. 6. The addition of PPG did not

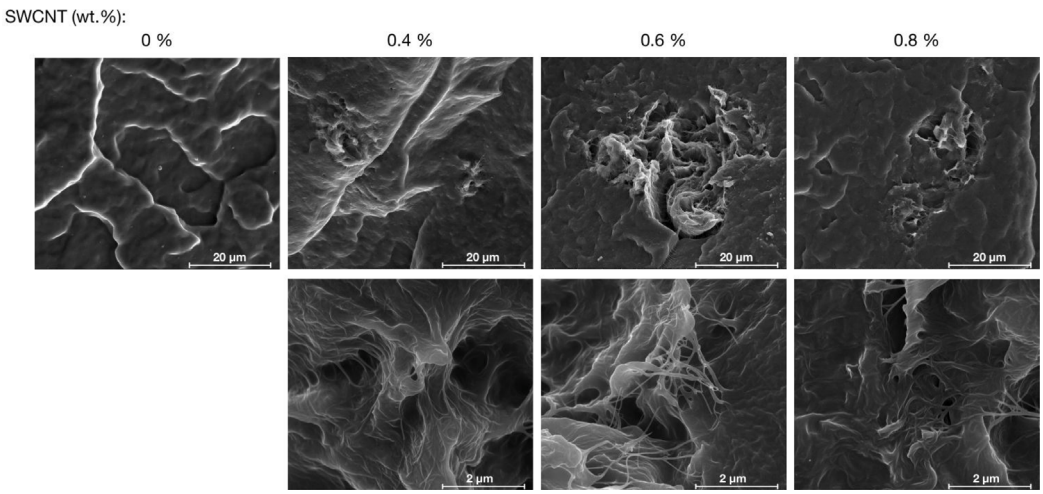

Fig. 6. Scanning electron micrographs (secondary electron mode) of melt-extruded TPU and composites with 0.4, 0.6, and 0.8 wt.% of SWCNT, collected at different magnifications.

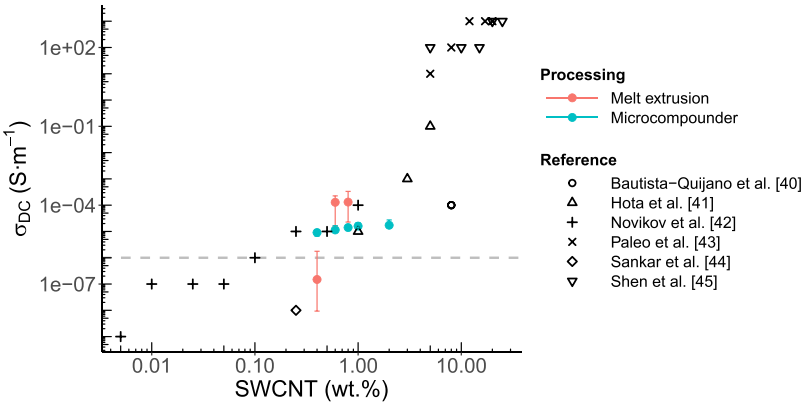

Fig. 7. Electrical conductivity (σ_{DC}) as a function of SWCNT weight percentage for composite filaments produced in a co-rotating intermeshing twin screw extruder (in red), in a microcompounder (in blue) and for composites reported in the literature, obtained through solvent casting (black). Error bars correspond to the maximum and minimum values obtained. (For interpretation of the references to color in this figure legend, the reader is referred to the web version of this article.)

seem to lead to phase differences within the matrix, demonstrating that a good compatibility between plasticizer and polymer exists. SWCNT are evenly distributed in the polymer, with some agglomerates present as depicted in Fig. 6, increasing in number with the increase in weight fraction of SWCNT (Figure A3a), as expected.

At 0.4 wt.% SWCNT load, the composites display an electrical conductivity (σ_{DC}) of 7.1×10^{-7} S m^{-1}, being fairly resistive. Composites prepared in a microcompounder (details in supplementary information, Table A2), with the same composition, present higher σ_{DC}, albeit remaining within the semi-conductive regime. However, increasing the SWCNT content up to 2 wt.%, while processing composites in a microcompounder, does not alter significantly the σ_{DC}, as depicted in Fig. 7 (blue data points). Moreover, Joule heating is not observed for these composites at both 60 and 90 V, whereas melt-extruded samples with lower loading heat up the surrounding matrix (supplementary data, Figure A4). Composites with 0.6 and 0.8 wt.% SWCNT content produced in the twin screw extruder show a drastic increase in σ_{DC} in relation to the lower loading, with measured values of 1.3×10^{-4} and 1.6×10^{-4} S m^{-1}. The ϕ_c of the melt-extruded composites occurs between 0.4 and 0.6 wt.% SWCNT content (Fig. 7, red data points).

According to the literature, solvent casting is the most common approach to fabricate TPU/SWCNT composites [40–45], with values for σ_{DC} ranging from 10^{-8} [42,44] up to 10^{2} S m^{-1} [43] and SWCNT content lower than 5 wt.%. These data are displayed in the scatter plot of Fig. 7 (in black). As expected, the σ_{DC} of the melt-extruded composite with 0.4 wt.% SWCNT falls below the reported results for similar wt.% since a better dispersion is usually obtained through solvent casting. However, for SWCNT loadings of 0.6 wt.% and above, the σ_{DC} of the melt-extruded composite filaments produced in this work are on the same order of magnitude of those reported in the literature for composites prepared through solvent casting, with SWCNT loads of 1 wt.% [42], 3 wt.% [41], and 8 wt.% [40]. Therefore, composites exhibiting electrical conductivity can be prepared by a melt mixing-process that is industry ready and more environmentally sustainable compared to solvent-based approaches.

3.2. Layered composite tapes

Since there were no significant differences between the MFI of composite filaments with 0.8 and 0.6 wt.% SWCNT (Table A1), and taking into consideration the measured σ_{DC}, TPU composite filaments with 0.6 wt.% SWCNT and 9 wt.% PPG (sTPU) were selected to produce multilayered tapes together with neat TPU, using the prototype device (Fig. 4). TPU and sTPU melts were fed to the device equipped with 1, 2, 3, and 4 LME. The resulting tapes, designated TPU/sTPU$_n$, where n corresponds to the number of LME used, with a thickness of ~ 700 µm, were collected in a water bath. The produced tapes, the number of LME used, and their average thickness are presented in Table 3.

The average thickness of the tapes has a tendency to increase with the increasing number of LME used (Table 3). Extrudate-swell develops at the exit of the extrusion die due to relaxation/flow reorientation phenomena of the melt, resulting from the change in surface characteristics

Table 3
Tapes produced with different number of LME, the initial melts (Melt A and Melt B) and average thickness of the produced tapes.

Sample designation	n° LME	Melt A	Melt B	Tape thickness (μm)
TPU/sTPU$_1$	1	TPU	sTPU	680 ± 12
TPU/sTPU$_2$	2			710 ± 25
TPU/sTPU$_3$	3			760 ± 20
TPU/sTPU$_4$	4			780 ± 20

(from flow between walls along the die to a free surface flow upon the exit). The magnitude of the phenomenon increases with increasing shear rate, since the latter induces molecular orientation. At constant total flow rate, as the number of LME increases, so does the average shear rate of the individual flow layers, since each will assume its own parabolic velocity profile. This induces a higher molecular orientation of each layer, therefore a higher relaxation at the die exit, leading to an increment of the overall extrudate-swell and, therefore, of the final thickness of the tape.

3.2.1. Morphology

The micrographs of the cross-sections of the composite tapes produced with the prototype device, with a different number of LME, are depicted in Fig. 8. The images suggest that the baker's transformation was applied. For the TPU/sTPU$_1$ tape, produced with 1 LME, the four layers of the neat TPU melt have an average thickness of 87.5 μm. This average layer size is close to the theoretically expected (Table 1), but both top and bottom TPU layers are not uniform, a variation of ±39.4 μm being calculated for the layer thickness distribution. The center layers are more even, with a median layer thickness of 89.2 μm. An average layer thickness of 99.5 μm was calculated for the layers composed of sTPU, with a variation of ± 41.9 μm. This non-uniformity of layer thickness is typical of static mixers [46]. Five layers of sTPU are observed, i.e., a very thin layer of around 6.4 μm is visible at the bottom. This results from secondary flows due to the viscoelastic nature of the melt, which may be exacerbated by the low aspect ratio of the channel, thus highlighting the complexity of flow in static mixers [47,48].

When using more than one LME, a layered profile is still observed. As expected, the change in rotation direction provided by the DenIncx mixer helps avoid Kolmogorov–Arnold–Moser (KAM) boundaries, and increasing the LME number results in a more stratified profile [28]. Layers become more even in thickness for TPU/sTPU$_3$ and TPU/sTPU$_4$, with disruptions being observed due to the presence of SWCNT agglomerates in the sTPU phase.

The statistical distribution of the measured agglomerates is reported in Table 4 for all tapes and melt-extruded sTPU composite. The median area (M) of SWCNT agglomerates tends to increase as the number of multipliers increases. A similar phenomenon occurs for the first quartile (Q_1).

Individual SWCNT stick together through van der Waals forces, forming nanotube "ropes", which further entangle to form stable and large agglomerates. As a consequence, extensive dispersion and complete elimination of agglomerates is difficult to attain. It is now well established that the dispersion of SWCNT agglomerates in polymer melts results from the contribution of two concurrent mechanisms, rupture and erosion. The former is rapid but requires sufficiently high hydrodynamic stresses, while erosion is a slow process that may develop even at low stresses [49,50]. Experimental evidence has demonstrated that high shear promotes extensive nanotube dispersion in the polymer melt, enhancing the composite's mechanical performance but hindering its electrical conductivity by eliminating conductive paths created by small agglomerates [51]. In the prototype device the shear rates generated are low (around 10 s^{-1}) and thus the corresponding shear stresses should also be limited. Therefore, erosion would be the only possible dispersion route. Under the layer formation conditions (low shear stress and short processing time), SWCNT dispersion will be limited to erosion, competing with SWCNT agglomerate relaxation that leads to re-agglomeration. As the number of LME increases, the duration of the flow increases proportionally, favoring re-agglomeration, i.e., the progressive "coalescence" of the existing agglomerates. Such phenomena have been previously reported for polypropylene/multi-walled carbon nanotubes [52], and polypropylene/graphite nanoplatelets [53] flowing at low shear rates. The data obtained for TPU/sTPU$_4$ is somewhat distinct from the remaining. As the number of individual layers increases, their thickness decreases, reaching orders of magnitude similar to that of the agglomerate sizes. This will certainly influence the flow behavior of the composite melt.

Table 4
Quartiles (Q_1, Median, and Q_3) of the measured SWCNT agglomerate's area (μm^2), and agglomerate count per sample.

Sample	Q_1 (μm^2)	M (μm^2)	Q_3 (μm^2)	Count
sTPU	2.67	4.62	11.17	280
TPU/sTPU$_1$	2.86	3.88	8.16	197
TPU/sTPU$_2$	3.88	11.23	47.77	59
TPU/sTPU$_3$	3.83	8.57	17.96	42
TPU/sTPU$_4$	6.48	13.57	51.34	100

Table 5
Mechanical properties of TPU, sTPU, and layered tapes produced with a different number of LME.

Sample	Young's Modulus (MPa)	Tensile strength (MPa)	Elongation at break (%)
TPU	8.3 ± 0.6	15.7 ± 0.9	1200 ± 50
sTPU	19.0 ± 5.6	4.1 ± 0.1	470 ± 80
TPU/sTPU$_2$	8.0 ± 1.3	5.7 ± 2.0	820 ± 390
TPU/sTPU$_3$	9.3 ± 0.3	6.1 ± 0.7	1110 ± 70
TPU/sTPU$_4$	9.4 ± 0.9	5.8 ± 0.7	1040 ± 130

TPU/sTPU$_1$ – 11.4 MPa (E), 8.7 MPa (tensile strength) and 1130% (elongation at break) based in one measurement.

Atomic Force Microscopy (AFM) using High Definition Kelvin Force Microscopy (HD-KFM) mode was performed on the cross-section of the TPU/sTPU$_3$ tape. The topography of the tape is represented in Fig. 9a. Areas with different surface roughness are visible in a stratified profile. The surface potential of the same area (Fig. 9b) indicates that the zones with higher surface roughness correspond to the sTPU phase, which has particles with high surface potential, the SWCNT. Phase images (Fig. 9c) indicate variations in the properties of the material. It is clear that the material responds differently to the tip in the different layers.

3.2.2. Mechanical properties

Representative stress–strain curves of TPU and sTPU films, and layered tapes are shown in Fig. 10. As expected, sTPU has the highest Young's modulus (E), while TPU presents the lowest, with values of 19.0 MPa and 8.3 MPa, respectively (Table 5). The tapes produced with small-scale LME present an intermediate E, around 10 MPa. Elongation at break is higher for TPU and lower for sTPU, which can be attributed to the presence of both SWCNT agglomerates and well dispersed, stiff SWCNT, contributing to reduced molecular mobility of the TPU polymer chains [42,54], resulting in lower ductility. However, layered tapes show a large elongation at break that approaches that of neat TPU, i.e., the elastomeric behavior is retained.

3.2.3. Electrical properties

The median values measured for σ_{DC} of the layered tapes processed with a different number of LME are plotted in Fig. 11. For comparison, the σ_{DC} values of the melt-extruded composite filaments, with 0.4 and 0.6 wt.% of SWCNT, are also plotted (0 LME). A nonparametric statistical analysis (Kruskal–Wallis test) was conducted to evaluate statistical differences between the median σ_{DC} of the composite with 0.6 wt.% SWCNT and the tapes. The null hypothesis was assessed (H_0:

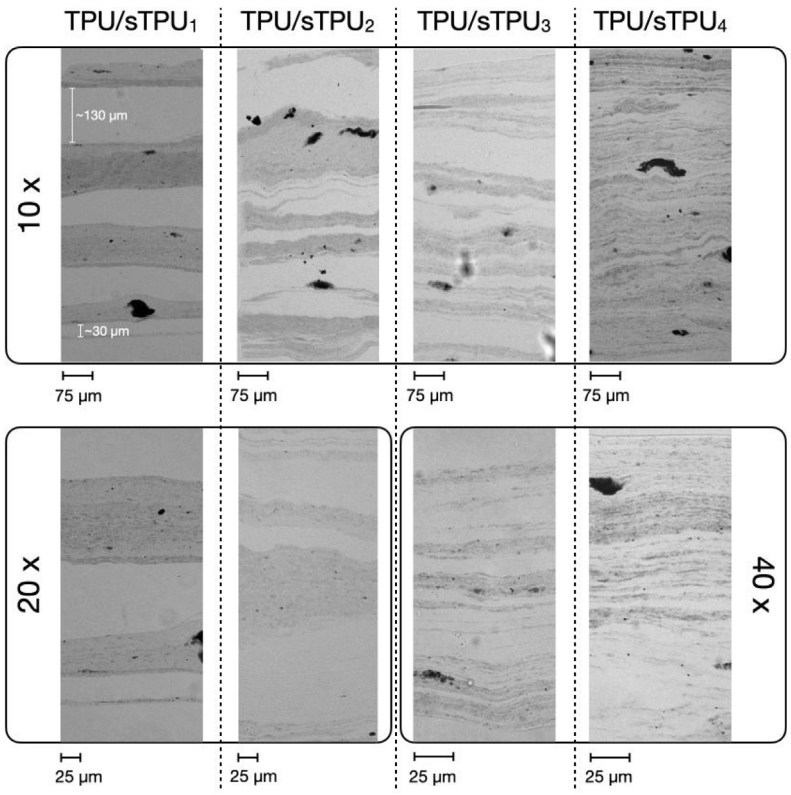

Fig. 8. Optical microscopy images of the cross-sections of the composite tapes, at different magnitudes (10x, 20x, and 40x), of the tapes produced with 1, 2, 3, and 4 LME.

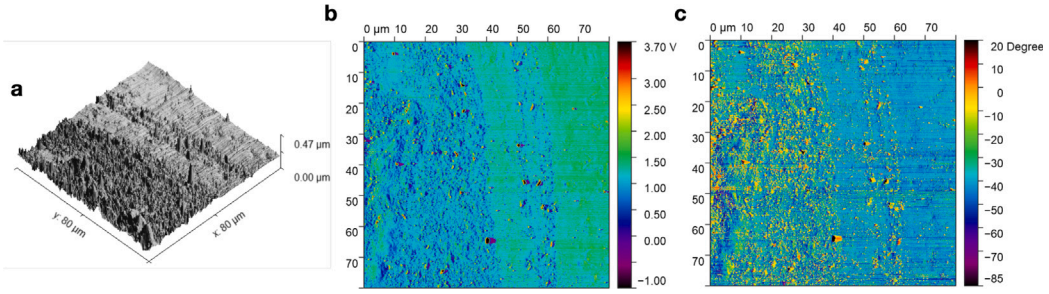

Fig. 9. AFM images: (a) topography, (b) surface potential, and (c) phase modes, of the cross-section of TPU/sTPU$_3$ tape.

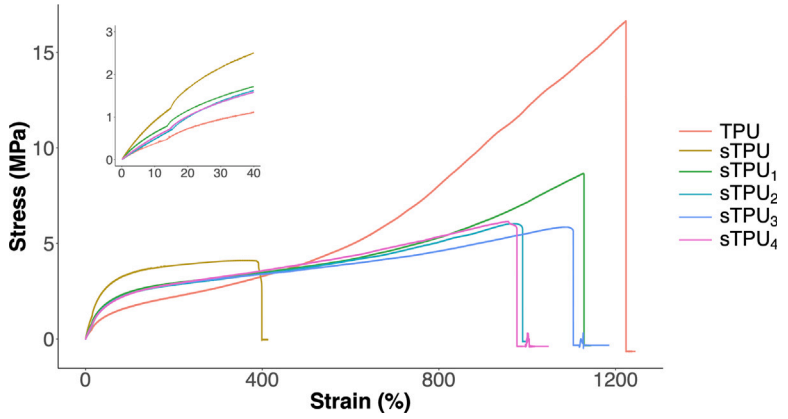

Fig. 10. Stress–strain curves of TPU, sTPU and TPU/sTPU tapes produced with a different number of LME. The inset shows the stress–strain curves from up to 40%. (For interpretation of the references to color in this figure legend, the reader is referred to the web version of this article.)

the population medians are equal) and the results obtained (H = 8.56, df = 4, *p*-value = 0.073) did not provide sufficient evidence to reject H_0, indicating no statistically significant differences in the median values of σ_{DC} for the 0.6 wt.% SWCNT composite and the layered

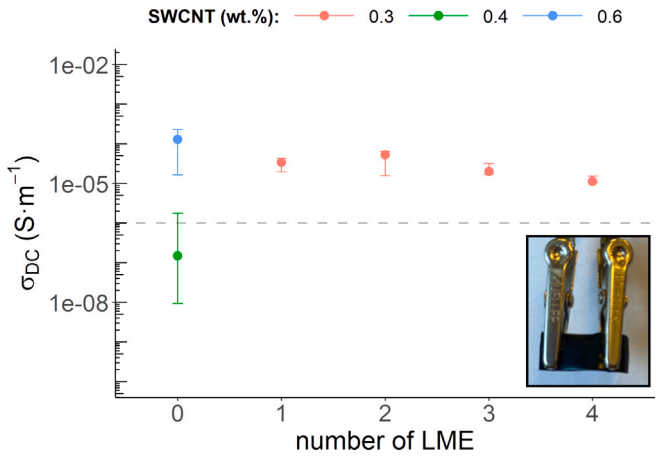

Fig. 11. σ_{DC} as a function of the number of LME, where 0 LME corresponds to the melt-extruded filament samples with 0.4 and 0.6 wt.% of SWCNT (green and blue, respectively). Error bars correspond to the maximum and minimum measured values. The inset displays the electrode clamps positioned on the tape specimen. (For interpretation of the references to color in this figure legend, the reader is referred to the web version of this article.)

tapes produced with different numbers of LME. Thus, by alternating sTPU and TPU layers in the prototype device, similar conductivity can be attained while halving the total SWCNT content. This result may reflect relaxion effects in the sTPU melt during the layer multiplication process, leading to nanotube re-agglomeration and enhancing the layer electrical conductivity. It should be mentioned that the presence of large SWCNT agglomerates, large enough to cross layers, bridges the layers through the tape thickness.

4. Conclusions

Composite filaments of TPU/SWCNT were successfully produced by melt-mixing in a small-scale twin screw extruder, presenting σ_{DC} in the range of 10^{-7} - 10^{-4} S m^{-1}. The use of PPG, as well as the shear stress applied in the extrusion process, were sufficient to achieve an electrical percolation threshold at 0.6 wt.%.

A prototype device composed of a series of small-scale melt multipliers was fabricated. The prototype allowed for the successful production of tapes composed of a different number of layers. TPU and sTPU were fed into the equipment to produce tapes with different stratification levels and alternating TPU and sTPU layers, depending on the number of LME used. The produced tapes have a total wt.% of 0.3 SWCNT in their composition. Their Young's modulus and tensile strength lies between that of neat TPU and sTPU. The tapes' elongation at break is similar to that of TPU, allowing them to withstanding larger deformation compared to sTPU. Moreover, the volume conductivity of the tapes is similar to that of sTPU. Therefore, it is possible to produce multifunctional materials exhibiting electrical conductivity and ductility with an elastomeric matrix containing only 0.3 wt.% of SWCNT.

The layered materials produced, with layers in the milli- and micrometer ranges, show great potential for applications in tissue engineering and soft robotics due to their ability of displaying adequate mechanical properties with an embedded conductive network.

CRediT authorship contribution statement

Mariana Martins da Silva: Writing – original draft, Visualization, Methodology, Investigation, Funding acquisition, Formal analysis, Data curation, Conceptualization. **Rui Ribeiro:** Investigation. **Ana Sofia Oliveira:** Investigation, Formal analysis. **Mariana Paiva Proença:** Writing – review & editing, Supervision, Resources. **Maria Conceição Paiva:** Writing – review & editing, Supervision, Resources, Methodology, Conceptualization. **José António Covas:** Writing – review & editing, Supervision, Resources, Conceptualization.

Declaration of competing interest

The authors declare that they have no known competing financial interests or personal relationships that could have appeared to influence the work reported in this paper.

Acknowledgments

The authors acknowledge the Portuguese Fundação para a Ciência e Tecnologia (FCT) for the funding through the Ph.D. grant with the reference 2020.05311.BD and through UID/05256: Instituto de Polímeros e Compósitos (IPC/UM). The authors acknowledge funding from the Spanish Ministerio de Ciencia, Innovación y Universidades under the projects PID2020-117024GB-C42 and PID2023-150853NB-C32. This work has also made use of the Spanish ICTS Network MICRONANOFABS. The authors thank the team of Extrusion, Compounding and Advanced Materials, from the Centre for Innovation in Polymer Engineering (PIEP), for the technical support provided with the microcompounder. The authors would also like to acknowledge Prof. Fernando Duarte and Prof. Sacha Mould for the support provided.

Appendix A. Supplementary data

Supplementary material related to this article can be found online at https://doi.org/10.1016/j.coco.2025.102448.

Data availability

Data will be made available on request.

References

[1] T. Ebbesen, H. Lezec, H. Hiura, J. Bennett, H. Ghaemi, T. Thio, Electrical conductivity of individual carbon nanotubes, Nature 382 (6586) (1996) 54–56, http://dx.doi.org/10.1038/382054a0.

[2] K. Hughes, K. Iyer, R. Bird, J. Ivanov, S. Banerjee, G. Georges, Q. Zhou, Review of Carbon Nanotube research and development: Materials and emerging applications, ACS Appl. Nano Mater. (2024) http://dx.doi.org/10.1021/acsanm.4c02721.

[3] M. da Silva, M. Proença, J. Covas, M. Paiva, Shape-memory polymers based on Carbon Nanotube composites, Micromachines 15 (6) (2024) 748, http://dx.doi.org/10.3390/mi15060748.

[4] G. Mittal, V. Dhand, K. Rhee, S. Park, W. Lee, A review on carbon nanotubes and Graphene as fillers in reinforced polymer nanocomposites, J. Ind. Eng. Chem. 21 (2015) 11–25, http://dx.doi.org/10.1016/j.jiec.2014.03.022.

[5] C. Li, E. Thostenson, T. Chou, Sensors and actuators based on carbon nanotubes and their composites: A review, Compos. Sci. Technol. 68 (2008) 1227–1249, http://dx.doi.org/10.1016/j.compscitech.2008.01.006.

[6] W. Bauhofer, J. Kovacs, A review and analysis of electrical percolation in carbon nanotube polymer composites, Compos. Sci. Technol. 69 (10) (2009) 1486–1498, http://dx.doi.org/10.1016/j.compscitech.2008.06.018.

[7] Z. Spitalsky, D. Tasis, K. Papagelis, C. Galiotis, Carbon nanotube-polymer composites: Chemistry, processing, mechanical and electrical properties, Prog. Polym. Sci. 35 (3) (2010) 357–401, http://dx.doi.org/10.1016/j.progpolymsci.2009.09.003.

[8] C. Min, X. Shen, Z. Shi, L. Chen, Z. Xu, The electrical properties and conducting mechanisms of carbon nanotube/polymer nanocomposites: A review, Polym.-Plast. Technol. Eng. 49 (2010) 1172–1181, http://dx.doi.org/10.1080/03602559.2010.496405.

[9] M. Moniruzzaman, K. Winey, Polymer nanocomposites containing carbon nanotubes, Macromolecules 39 (16) (2006) 5194–5205, http://dx.doi.org/10.1021/ma060733p.

[10] P. Ma, N. Siddiqui, G. Marom, J. Kim, Dispersion and functionalization of carbon nanotubes for polymer-based nanocomposites: A review, Compos. Part A- Appl. Sci. Manuf. 41 (10) (2010) 1345–1367, http://dx.doi.org/10.1016/j.compositesa.2010.07.003.

[11] J. Banerjee, K. Dutta, Melt-mixed carbon nanotubes/polymer nanocomposites, Polym. Compos. 40 (12) (2019) 4473–4488, http://dx.doi.org/10.1002/pc.25334.

[12] N. Hocine, C. Miranda, S. Nauman, A. Langlet, Electrical properties of elastomer-based composites reinforced with carbon nanotubes-A review, Polym. Adv. Technol. 35 (2024) http://dx.doi.org/10.1002/pat.6299.

[13] S. Srivastava, N. Kotov, Composite Layer-by-Layer (LBL) Assembly with inorganic nanoparticles and nanowires, Acc. Chem. Res. 41 (2008) 1831–1841, http://dx.doi.org/10.1021/ar8001377.
[14] A. de Leon, Q. Chen, N. Palaganas, J. Palaganas, J. Manapat, R. Advincula, High performance polymer nanocomposites for additive manufacturing applications, React. Funct. Polym. 103 (2016) 141–155, http://dx.doi.org/10.1016/j.reactfunctpolym.2016.04.010.
[15] X. Qi, J. Yang, N. Zhang, T. Huang, Z. Zhou, I. Kuhnert, P. Potschke, Y. Wang, Selective localization of carbon nanotubes and its effect on the structure and properties of polymer blends, Prog. Polym. Sci. 123 (2021) http://dx.doi.org/10.1016/j.progpolymsci.2021.101471.
[16] Y. Gao, O. Picot, W. Tu, E. Bilotti, T. Peijs, Multilayer coextrusion of graphene polymer nanocomposites with enhanced structural organization and properties, J. Appl. Polym. Sci. 135 (13) (2018) http://dx.doi.org/10.1002/app.46041.
[17] G. Miquelard-Garnier, A. Guinault, D. Fromonteil, S. Delalande, C. Sollogoub, Dispersion of carbon nanotubes in polypropylene via multilayer coextrusion: Influence on the mechanical properties, Polymer 54 (16) (2013) 4290–4297, http://dx.doi.org/10.1016/j.polymer.2013.06.007.
[18] Z. Li, A. Olah, E. Baer, Micro- and nano-layered processing of new polymeric systems, Prog. Polym. Sci. 102 (2020) http://dx.doi.org/10.1016/j.progpolymsci.2020.101210.
[19] M. Ponting, A. Hiltner, E. Baer, Polymer nanostructures by Forced Assembly: Process, structure, and properties, Layer. Nanostructures - Polym. Improv. Prop. 294-I (2010) 19–+, http://dx.doi.org/10.1002/masy.201050803.
[20] X. Zhang, Y. Xu, X. Zhang, H. Wu, J. Shen, R. Chen, Y. Xiong, J. Li, S. Guo, Progress on the layer-by-layer assembly of multilayered polymer composites: Strategy, structural control and applications, Prog. Polym. Sci. 89 (2019) 76–107, http://dx.doi.org/10.1016/j.progpolymsci.2018.10.002.
[21] J. Carr, D. Langhe, M. Ponting, A. Hiltner, E. Baer, Confined crystallization in polymer nanolayered films: A review, J. Mater. Res. 27 (10) (2012) 1326–1350, http://dx.doi.org/10.1557/jmr.2012.17.
[22] J. Wang, D. Adami, B. Lu, C. Liu, A. Maazouz, K. Lamnawar, Multiscale structural evolution and its relationship to Dielectric properties of micro-/nano-layer Coextruded PVDF-HFP/PC films, Polymers 12 (11) (2020) http://dx.doi.org/10.3390/polym12112596.
[23] A. Bironeau, T. Salez, G. Miquelard-Garnier, C. Sollogoub, Existence of a critical layer thickness in PS/PMMA nanolayered films, Macromolecules 50 (10) (2017) 4065–4074, http://dx.doi.org/10.1021/acs.macromol.7b00176.
[24] P. Neerincx, M. Hofmann, O. Gorodetskyi, K. Feldman, J. Vermant, H. Meijer, One-step creation of hierarchical fractal structures, Polym. Eng. Sci. 61 (4) (2021) 1257–1269, http://dx.doi.org/10.1002/pen.25677.
[25] A. Stroock, S. Dertinger, A. Ajdari, I. Mezic, H. Stone, G. Whitesides, Chaotic mixer for microchannels, Science 295 (5555) (2002) 647–651, http://dx.doi.org/10.1126/science.1066238.
[26] D. Kim, S. Lee, T. Kwon, S. Lee, A barrier embedded chaotic micromixer, J. Micromech. Microeng. 14 (6) (2004) 798–805, http://dx.doi.org/10.1088/0960-1317/14/6/006.
[27] D. Kim, S. Lee, T. Kwon, C. Ahn, A serpentine laminating micromixer combining splitting/recombination and advection, Lab on a Chip 5 (7) (2005) 739–747, http://dx.doi.org/10.1039/b418314b.
[28] P. Neerincx, R. Denteneer, S. Peelen, H. Meijer, Compact mixing using multiple splitting, stretching, and recombining flows, Macromol. Mater. Eng. 296 (3–4) (2011) 349–361, http://dx.doi.org/10.1002/mame.201000338.
[29] P. Harris, J. Patz, B. Huntington, R. Bonnecaze, D. Meltzer, J. Maia, Improved interfacial surface generator for the co-extrusion of micro- and nanolayered polymers, Polym. Eng. Sci. 54 (3) (2014) 636–645, http://dx.doi.org/10.1002/pen.23597.
[30] J. Dooley, J. Robacki, S. Jenkins, P. Lee, R. Wrisley, Producing microlayer blown film structures using layer multiplication and unique die technology, in: Annual Technical Conference - ANTEC, 2011.
[31] M. Ponting, T. Burt, L. Korley, J. Andrews, A. Hiltner, E. Baer, Gradient multilayer films by forced Assembly Coextrusion, Ind. Eng. Chem. Res. 49 (23) (2010) 12111–12118, http://dx.doi.org/10.1021/ie100321h.
[32] A. Ranade, A. Hiltner, E. Baer, D. Bland, Structure-property relationships in coextruded foam/film microlayers, J. Cell. Plast. 40 (6) (2004) 497–507, http://dx.doi.org/10.1177/0021955x04048425.
[33] M. Silva, P. Lopes, Y. Li, P. Pötschke, F. Ferreira, M. Paiva, Polylactic acid/carbon nanoparticle composite filaments for sensing, Appl. Sci. 11 (6) (2021) 2580, http://dx.doi.org/10.3390/app11062580.
[34] P. Neerincx, Design to Realize Integrated Polymer Products (Ph.D. thesis), Technische Universiteit Eindhoven, 2012, http://dx.doi.org/10.6100/IR732932.
[35] C. Schneider, W. Rasband, K. Eliceiri, NIH image to ImageJ: 25 years of image analysis, Nature Methods 9 (7) (2012) 671–675, http://dx.doi.org/10.1038/nmeth.2089.
[36] R. Team, RStudio: Integrated development environment for R, 2020, URL http://www.rstudio.com/.
[37] H. Wickham, R. François, L. Henry, K. Müller, dplyr: A Grammar of data manipulation, 2022, URL https://CRAN.R-project.org/package=dplyr.
[38] H. Wickham, M. Averick, J. Bryan, W. Chang, L. McGowan, R. François, G. Grolemund, A. Hayes, L. Henry, J. Hester, M. Kuhn, T. Pedersen, E. Miller, S. Bache, K. Müller, J. Ooms, D. Robinson, D. Seidel, V. Spinu, K. Takahashi, D. Vaughan, C. Wilke, K. Woo, H. Yutani, Welcome to the tidyverse, J. Open Source Softw. 4 (2019) 1686, http://dx.doi.org/10.21105/joss.01686.
[39] H. Wickham, ggplot2: Elegant Graphics for Data Analysis, Springer-Verlag, New York, 2016, URL https://ggplot2.tidyverse.org.
[40] J. Bautista-Quijano, F. Aviles, J. Cauich-Rodriguez, R. Schonfelder, A. Bachmatiuk, T. Gemming, M. Rummeli, Tensile piezoresistivity and disruption of percolation in singlewall and multiwall carbon nanotube/polyurethane composites, Synth. Met. 185 (2013) 96–102, http://dx.doi.org/10.1016/j.synthmet.2013.09.041.
[41] N. Hota, B. Sahoo, Single-walled carbon nanotube filled thermoplastic polyurethane nanocomposites: Influence of ionic liquid on dielectric properties, Mater. Today Proc. 41 (2021) 216–222, http://dx.doi.org/10.1016/j.matpr.2020.08.713.
[42] I. Novikov, D. Krasnikov, A. Vorobei, Y. Zuev, H. Butt, F. Fedorov, S. Gusev, A. Safonov, E. Shulga, S. Konev, I. Sergeichev, S. Zhukov, T. Kallio, B. Gorshunov, O. Parenago, A. Nasibulin, Multifunctional elastic nanocomposites with extremely low concentrations of single-walled carbon nanotubes, ACS Appl. Mater. Interfaces 14 (16) (2022) 18866–18876, http://dx.doi.org/10.1021/acsami.2c01086.
[43] A. Paleo, Y. Martinez-Rubi, B. Krause, P. Pöetschke, M. Jakubinek, B. Ashrafi, C. Kingston, Carbon nanotube-polyurethane composite sheets for flexible Thermoelectric materials, ACS Appl. Nano Mater. 6 (19) (2023) 17986–17995, http://dx.doi.org/10.1021/acsanm.3c03247.
[44] R. Sankar, K. Meera, A. Mandal, S. Jaisankar, Thermoplastic polyurethane/single-walled carbon nanotube composites with low electrical resistance surfaces, High Perform. Polym. 25 (2) (2013) 135–146, http://dx.doi.org/10.1177/0954008312459545.
[45] Y. Shen, Y. Wang, Z. Luo, B. Wang, Durable, sensitive, and wide-range wearable pressure sensors based on Wavy-Structured flexible conductive composite film, Macromol. Mater. Eng. 305 (8) (2020) http://dx.doi.org/10.1002/mame.202000206.
[46] H. Meijer, M. Singh, P. Anderson, On the performance of static mixers: A quantitative comparison, Prog. Polym. Sci. 37 (10) (2012) 1333–1349, http://dx.doi.org/10.1016/j.progpolymsci.2011.12.004.
[47] J. Dooley, Viscoelastic Flow Effects in Multilayer Polymer Coextrusion (Ph.D. thesis), Technische Universiteit Eindhoven, 2002, http://dx.doi.org/10.6100/IR555718.
[48] B. Lu, H. Zhang, A. Maazouz, K. Lamnawar, Interfacial phenomena in multi-micro-/nanolayered polymer coextrusion: A Review of fundamental and Engineering aspects, Polymers 13 (3) (2021) http://dx.doi.org/10.3390/polym13030417.
[49] G. Kasaliwal, T. Villmow, S. Pegel, P. Pötschke, 4 - Influence of material and processing parameters on carbon nanotube dispersion in polymer melts, in: T. McNally, P. Pötschke (Eds.), Polymer–Carbon Nanotube Composites, in: Woodhead Publishing Series in Composites Science and Engineering, Woodhead Publishing, 2011, pp. 92–132, http://dx.doi.org/10.1533/9780857091390.1.92.
[50] T. McNally, P. Pötschke, Polymer-carbon nanotube composites: Preparation, properties and applications, Mater. Today 14 (10) (2011) 502, http://dx.doi.org/10.1016/S1369-7021(11)70215-2.
[51] S. Pegel, P. Pötschke, G. Petzold, I. Alig, S.M. Dudkin, D. Lellinger, Dispersion, agglomeration, and network formation of multiwalled carbon nanotubes in polycarbonate melts, Polymer 49 (4) (2008) 974–984, http://dx.doi.org/10.1016/j.polymer.2007.12.024.
[52] S. Jamali, M. Paiva, J. Covas, Dispersion and re-agglomeration phenomena during melt mixing of polypropylene with multi-wall carbon nanotubes, Polym. Test. 32 (4) (2013) 701–707, http://dx.doi.org/10.1016/j.polymertesting.2013.03.005.
[53] R. Santos, C. Vilaverde, E. Cunha, M. Paiva, J. Covas, Probing dispersion and re-agglomeration phenomena upon melt-mixing of polymer-functionalized graphite nanoplates, Soft Matter 12 (1) (2016) 77–86, http://dx.doi.org/10.1039/c5sm01366f.
[54] R. Sattar, A. Kausar, M. Siddiq, Advances in thermoplastic polyurethane composites reinforced with carbon nanotubes and carbon nanofibers: A review, J. Plast. Film Sheeting 31 (2015) 186–224, http://dx.doi.org/10.1177/8756087914535126.